

Microstructure and thermodynamic investigation of Ni–Ti system produced by mechanical alloying

A. Rostami^a, G.A. Bagheri^{b,*}, S.K. Sadrnezhaad^b

^a School of Electrical and Computer Engineering, University of Tehran, P.O. Box: 1439957131, Tehran, Iran

^b Department of Materials Science and Engineering, Sharif University of Technology, Azadi Ave., P.O. Box: 11155-9466, Tehran, Iran

ARTICLE INFO

Keywords:

Amorphous materials
Miedema's semi empirical method
NiTi intermetallic compound
Mechanical alloying

ABSTRACT

In this study, an equiatomic mixture of Ni and Ti powders has been mechanically milled for 180 h in a planetary mill in order to study the product phase of milling process. Miedema's semi empirical method has been used in order to calculate the energy of solid solution and amorphous phases and the effect of defects like dislocations and grain boundaries have been considered in this thermodynamic approach. The results showed that amorphous phase is more stable than solid solution after mechanical milling process. It seems these results are in contrast with Mousavi et al. [1] results but there are some points that we should consider in this approach. Applying of common tangent rule and considering the grain boundaries and dislocation energies in this thermodynamic approach lead to anticipating of amorphous phase as the stable phase after mechanical alloying process while lack of considering these terms in Mousavi et al. study led to different results. The milled powders has been heat treated at 950°C for 20 min and finally, XRD and SEM analysis have been performed in order to evaluate experimental phases and compare experimental and theoretical results. Crystallite size and lattice strain have been calculated using Williamson-Hall equation and XRD patterns.

1. Introduction

NiTi intermetallic compound (nitinol) has been found as a proper material for applications in medical and engineering areas due to its particular properties like shape memory effect, super elasticity, biocompatibility, vibration dumping and good erosion resistance [1–4]. The shape memory effect of this material is due to the transformation between high temperature austenite phase (B2) and low temperature martensite phase (B19'). Different procedures such as casting, powder metallurgy, self-propagating high temperature synthesis and mechanical alloying have been used in order to produce NiTi [5]. Conventional methods like melting and casting are energy consuming and hard to control the segregation of elements during solidification. Mechanical alloying is a solid state technique for producing super saturated solid solutions, amorphous materials, metal based nanocomposites and oxide dispersion-strengthened materials in temperatures far below melting temperatures of constituents. In this technique, repeated collisions of balls together leads to energy transferring to the trapped particles between two balls and plastic deformation of powder particles [6]. The density of lattice defects like dislocations and grain boundaries increases during milling process, and solid solution or amorphous phase will produce depend on Gibbs free energy of system.

Miedema manner is a semi empirical method for calculating the Gibbs free energy of solid solution and amorphous phase of binary or ternary solid systems considering three chemical, structural and elastic terms of enthalpy [7–10]. But original Miedema thermodynamic procedure is not suitable for prediction of mechanical milling product phases because of high amounts of defects especially dislocations and grain boundaries in the lattice of milled samples. Needless to say these defects increase the Gibbs free energy of system while original Miedema manner does not count these energies in the calculation of Gibbs free energy. So, we calculated Gibbs free energy of Ni–Ti system using Miedema approach and then the terms of dislocations and grain boundaries energies have been considered in final Gibbs free energy of system. Finally, the results of thermodynamic approach have been compared with experimental results.

2. Experimental procedure

An equiatomic mixture of Ni (99.9% purity and particle size less than 106 μ) and Ti (99% purity and particle size less than 20 μ) powders was charged into a planetary mill and milling process was performed for 180 h under argon atmosphere in order to prevent undesired reactions of powders. The milling speed and ball to powder weight ratio

* Corresponding author.

E-mail addresses: abrostami@ut.ac.ir (A. Rostami), gh.a.bagheri65@gmail.com (G.A. Bagheri), sadrnezh@sharif.edu (S.K. Sadrnezhaad).

have been chosen 180 RPM and 10:1 respectively. 1 wt.% Stearic acid was used as process control agent (PCA) in order to inhibit agglomeration of powders and sticking of powders to the wall of the container and balls. The heat treatment of milled powders has been done at 950°C for 20 min under argon atmosphere.

X-ray diffraction (XRD) analysis of milled powders and heat treated powders were performed by X-ray Diffractometer (EQuniox 3000, Inel, France) with $\text{CuK}\alpha$ ($\lambda = 1.54 \text{ \AA}$) radiation. Scanning electron microscope (SEM, LEO 1400) with energy dispersive X-ray spectrometer (EDS) and FESEM were used to study the morphology and composition of the powders after different milling times.

3. Results and discussion

3.1. Thermodynamic analysis

The Gibbs free energy formation of A-B solution can be calculated by equation (1) [11]:

$$\Delta G^s = \Delta H_m^s - T\Delta S^s \quad (1)$$

Where ΔH_m^s and ΔS^s are enthalpy and entropy of mixing respectively. T is the temperature of solid solution formation. It is noticeable that the constituent energies are in the standard state. ΔS^s has been considered equal to the entropy of mixing of ideal solution, then it can be calculated by equation (2) as follows [11]:

$$\Delta S^s = -R(x_A \cdot \ln x_A + x_B \cdot \ln x_B) \quad (2)$$

(R) and (x) are universal gas constant and molar fraction of constituents respectively.

According to Miedema's semi-empirical method, solid solution enthalpy of formation consists of three contribution terms [7–10]:

$$\Delta H^s = \Delta H_{\text{chemical}} + \Delta H_{\text{elastic}} + \Delta H_{\text{structural}} \quad (3)$$

$\Delta H_{\text{chemical}}$ is the chemical contribution of enthalpy which is the same for both solid and liquid solutions. $\Delta H_{\text{elastic}}$ term is related to size mismatch between two or more constituents and finally $\Delta H_{\text{structural}}$ contribution is related to crystal structures of solvent and solute and the difference in the number of valence electrons [12,13]. The amount of $\Delta H_{\text{chemical}}$ in a binary system can be determined by the following equation [7–10]:

$$\Delta H_{\text{chemical}} = \frac{2Pf(C^S)(x_A V_A^{2/3} + x_B V_B^{2/3})}{(n_{ws}^A)^{-1/3} + (n_{ws}^B)^{-1/3}} \times [-(\Delta\Phi)^2 + \frac{Q}{P}(\Delta n_{ws}^{1/3})^2 - \frac{S}{P}] \quad (4)$$

where Φ^s , n_{ws} and (V) are work function, electron density and molar volume respectively, (P) and (Q) are empirical constants and x_A and x_B are mole fractions of constituents. $f(C^S)$ or concentration function can be achieved by equations (5) and (6) for solid solutions [7–10]:

$$f(C^S) = C_A^S C_B^S \quad (5)$$

$$C_A^S = \frac{x_A V_A^{2/3}}{x_A V_A^{2/3} + x_B V_B^{2/3}}, \text{ and } C_B^S = \frac{x_B V_B^{2/3}}{x_A V_A^{2/3} + x_B V_B^{2/3}} \quad (6)$$

The elastic term of enthalpy can be calculated by equation (7) [3,7]:

$$\Delta H_{\text{elastic}} = x_A x_B (x_A \Delta E_{A \text{ in } B} + x_B \Delta E_{B \text{ in } A}) \quad (7)$$

$\Delta E_{A \text{ in } B}$ is the induced elastic energy due to dissolving of A atoms in B and conversely about $\Delta E_{B \text{ in } A}$. These amounts can be determined by equation (8) [3,7]:

$$\Delta E_{A \text{ in } B} = \frac{2K_A \cdot G_B (\Delta V)^2}{3K_A \cdot V_B + 4G_B V_A}, \Delta E_{B \text{ in } A} = \frac{2K_B \cdot G_A (\Delta V)^2}{3K_B \cdot V_A + 4G_A V_B} \quad (8)$$

(K) and (G) are bulk and shear modulus respectively.

The structural term of enthalpy is related to binary alloys of both transition metals like Ni–Ti which have partly filled d-shells. If we assume that solid solution atoms form a common d-bond, we can estimate the structural enthalpy of solid solution using the empirical curve

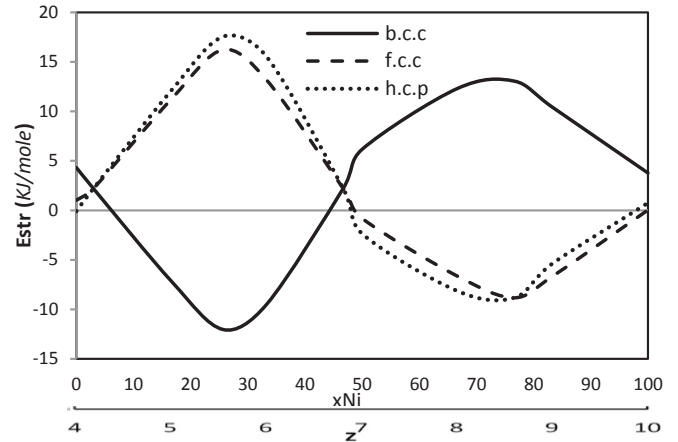


Fig. 1. The energy of lattice stability of b.c.c, f.c.c and h.c.p structures versus nickel concentration and \bar{z} .

of E_{str} (the energy of lattice stability) for three main crystal structures (f.c.c, h.c.p and b.c.c) (Fig. 1). Then $\Delta H_{\text{structural}}$ can be determined using equations (9) and (10) [8,9,12].

$$\Delta H_{\text{structural}} = E^{\text{str}}(\bar{z}) - E^{\text{ref}}(\bar{z}) \quad (9)$$

$$\bar{z} = x_A z_A + x_B z_B \quad (10)$$

where z_A and z_B are the valence electrons of A and B atoms, $E^{\text{str}}(\bar{z})$ is the lowest amount of $E_{f.c.c}^{\text{str}}$, $E_{b.c.c}^{\text{str}}$ and $E_{h.c.p}^{\text{str}}$ in Fig. 1 and $E^{\text{ref}}(\bar{z})$ is the linear interpolation between the E^{str} of pure constituents.

The elastic and structural contribution terms of enthalpy play no role in amorphous alloys because there is no crystal structure and atoms can rearrange themselves in such a way to relax the elastic energy. The enthalpy of amorphous alloys can be determined by equation (11) [9,12]:

$$\Delta H_{\text{amorphous}} = \Delta H_{\text{chemical}} + \alpha T_{\text{fuse}} \quad (11)$$

where $\alpha = 3.5 \text{ J mol}^{-1} \text{ K}^{-1}$ and T_{fuse} is defined by equation (12) [3,7]:

$$T_{\text{fuse}} = x_A T_m^A + x_B T_m^B \quad (12)$$

T_m^A and T_m^B are the melting temperatures of elements A and B, respectively.

Substituting of parameters of Table 1 into above equations leads to Fig. 2(a) and (b) curves for chemical, structural and elastic enthalpies and solid solution and amorphous Gibbs free energy of Ni–Ti system at 298 K. This temperature was selected in order to compare the results with Mousavi et al. curves. The both amorphous and solid solution Gibbs free energy curves shift in the same way by increasing the temperature which means the classic Miedema's semi empirical approach anticipates the solid solution as the stable phase even in higher temperatures.

It seems that amorphous phase has lower energy compared to solid solution in the middle area of curves but we should notice that applying of common tangent rule [11] in solid solution curve (as we can see in the area of 28–63 at.% Ni) anticipates two stable phases with 28 at.% Ni and 63 at.% Ni instead of amorphous phase.

But this thermodynamic approach is suitable for equilibrium processes while mechanical alloying is a non-equilibrium process and the

Table 1
Used parameters for calculating of enthalpy and Gibbs free energy [3,14].

Element	V_m (cm ³ /mole)	K (GPa)	G (GPa)	n_{ws} (10 ²³ e/cm ³)	Φ^s (V)
Ni	6.6	177.3	76.0	5.36	5.2
Ti	10.6	108.4	45.6	3.18	3.65

$$P = 14.1 \text{ kJ V}^{-2} \text{ cm}^{-1}, S/P = 0 \text{ and } Q/P = 9.4.$$

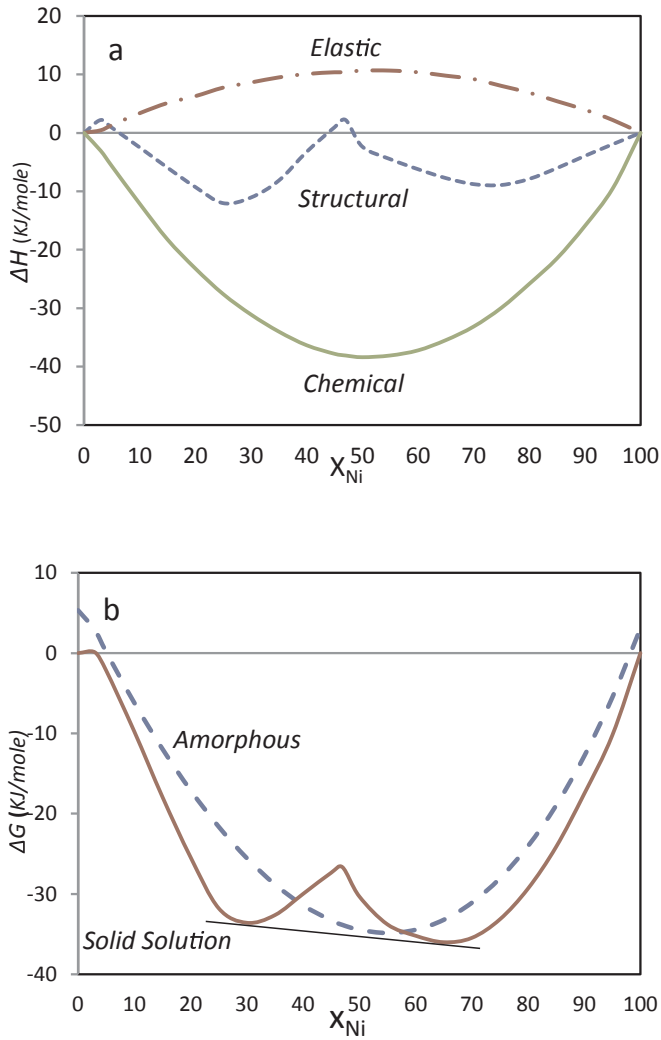


Fig. 2. (a) Chemical, elastic and structural curves of enthalpy and (b) solid solution and amorphous curves of Gibbs free energy of Ni–Ti system based on Miedema approach.

effect of induced energy by milling process which emerges in the form of lattice defects should be added. In other words the terms of grain boundaries and dislocations should be considered in calculations of Gibbs free energy of solid solution especially for products of milling process which have fine microstructure with high dislocations density. The effect of grain boundaries energy (ΔG^{γ}) and dislocations energy (ΔG^{dis}) can be considered in the Gibbs free energy of crystalline solid solution using the following equations [15–19]:

$$\Delta G^{crys.} = \Delta G^s + \Delta G^{\gamma} + \Delta G^{dis} \quad (13)$$

$$\Delta G^{\gamma} = 4\gamma \frac{V_m}{d} \quad (14)$$

where γ (0.87 J/m² for Ni [20]), V_m and (d) are grain boundary energy, molar volume and average grain size respectively.

$$\Delta G^{dis} = \zeta \rho V_m \quad (15)$$

$$\zeta = \left(\frac{Gb^2}{4\pi} \right) \ln \left(\frac{R_e}{b} \right) \quad (16)$$

$$\rho = \frac{2\sqrt{3}\epsilon^2}{(d \times b)} \quad (17)$$

where ζ is elastic energy of dislocation per unit length, ρ is dislocation density, ϵ is lattice strain, (d) is crystallite size and (b) is burgers vector.

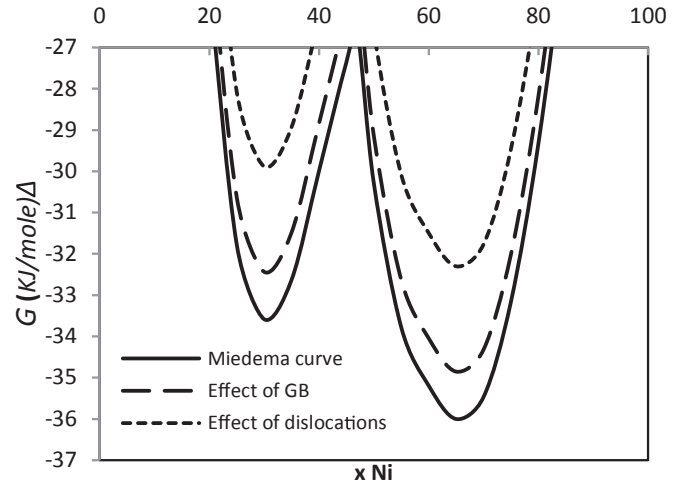


Fig. 3. The effect of dislocations and grain boundaries on the Gibbs free energy curve.

R_e is the outer cut off radius which can be considered as crystallite size in nanostructured materials.

The effects of grain boundaries and dislocations on the calculated Gibbs free energy of solid solution by Miedema manner have been shown in Fig. 3. The crystallite size and lattice strain were considered 20 nm and 0.5% in these curves respectively. These amounts are related to 110 h milled specimen (based on Fig. 7) and it seems no further refinement occurs by extra milling. So, we considered 20 nm and 0.5% as the final crystallite size and lattice strain of Ni–Ti milling system.

It is clear that defects boost the Gibbs free energy due to higher energy of these regions compared with defect free specimen. Fig. 4 compares Gibbs free energies of nanostructured solid solution (20 nm crystallite size and 0.5% lattice strain) with amorphous one. It can be seen that the amorphous phase has lower Gibbs free energy and is more stable than solid solution phase in milled specimens.

It seems that using the same thermodynamic route has led to different results in present work with Mousavi et al. work [3]. They anticipated solid solution (specifically B2 structure) as stable phase while the prediction of this work is amorphous as the phase with lower Gibbs free energy compared with crystalline phase. In order to respond to this contradiction we should mention some points in Mousavi et al. thermodynamic procedure in continue.

First, it is evident that the amount of the elastic enthalpy of a solid solution increases as the difference between the atomic sizes of the constituting elements increases. Due to the large atomic size mismatch

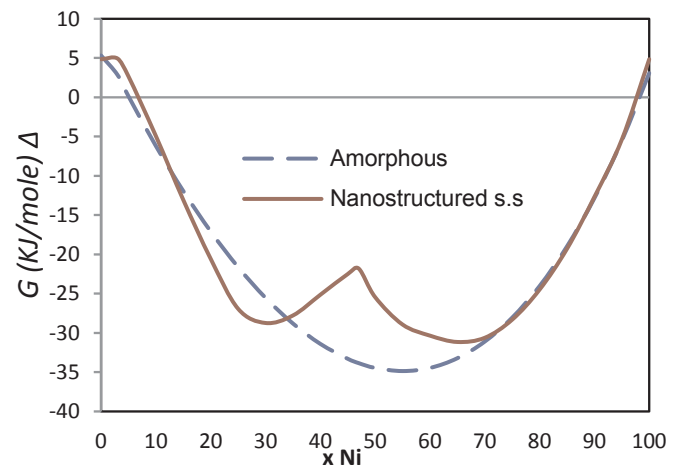


Fig. 4. Amorphous and nanostructured solid solution Gibbs free energy curves considering dislocations and grain boundaries energies.

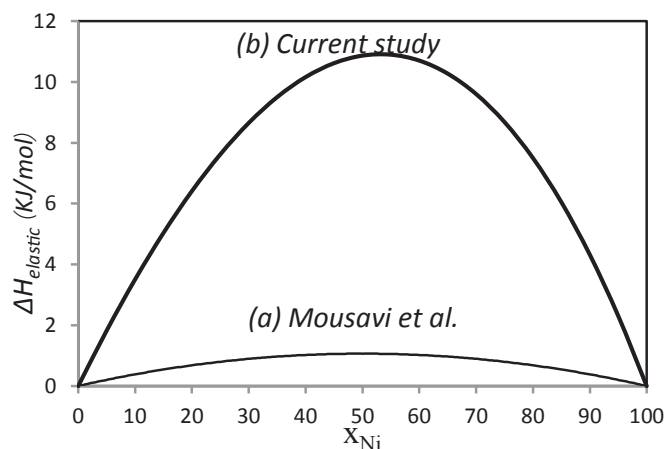


Fig. 5. Difference between calculated elastic enthalpy in Mousavi et al. article with ours.

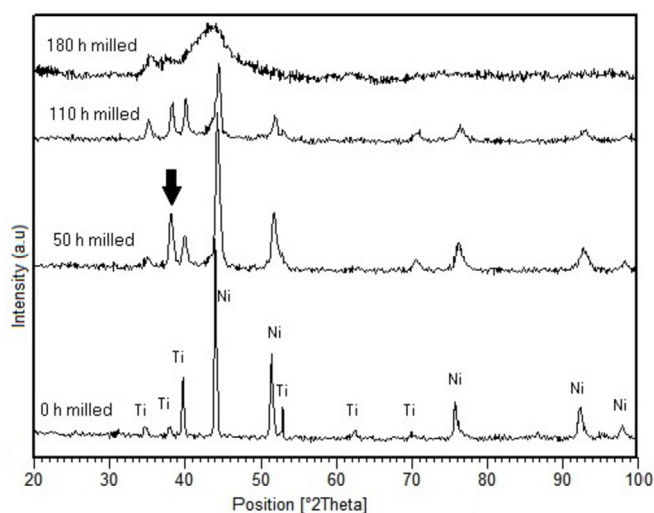


Fig. 6. XRD patterns of milled powders at different milling times.

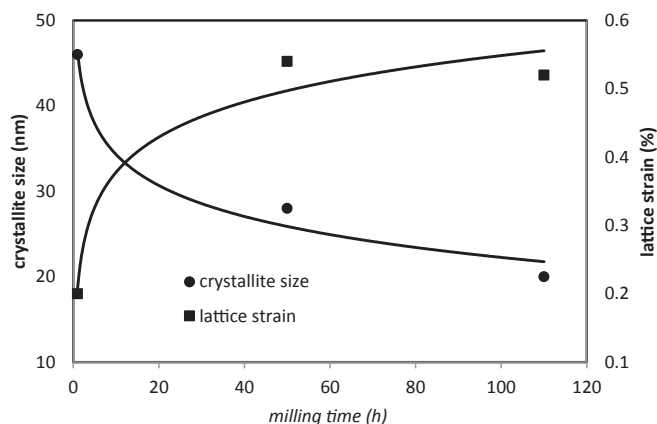


Fig. 7. Variations of crystallite size and lattice strain calculated by Williamson-Hall equation versus milling time.

which is present between nickel and titanium ($\sim 14\%$), one can readily predict the existence of a considerable lattice strain in the Ni–Ti solid solution. Nevertheless, Mousavi et al. [3] have reported negligible amounts of strain energy, less than 1 kJ/mol, for all Ni–Ti solid solution concentrations. Hence, they have considered no major contribution for the elastic part of the final Ni–Ti solid solution enthalpy in their

calculations. We have obtained much larger amounts of elastic enthalpies as shown in Fig. 1 using the same equation (equations (7) and (8)) and the same amounts for V_m , K and G parameters (Table 1) which have been employed by Mousavi et al. [3]. At 50 at.% Ni, for instance, our calculated elastic enthalpy is 10.8 kJ/mol, while that of Mousavi et al. is 1.08 kJ/mol (Fig. 5).

Second, the common tangent rule is a principal rule for prediction of stable phases [11]. Apparently, Mousavi et al. have not applied this rule on their results (see Fig. 4 in Ref. [3]). Hence, they have incorrectly reported the disordered phase of the B2–NiTi, i.e. a single solid solution while by applying the common tangent rule between the two minima of solid solution curve (see Fig. 2(b)), one recognizes that the stable phases are two solid solutions: (i) having 28 atom% Ni, and (ii) having 63 atom% Ni, in the 28–63 atom% Ni range. Thus, for 50 atom% Ni, what original Miedema model predicts are the two aforesaid phases, not a single one.

The last point about Mousavi et al. work is that the effect of grain boundaries energy and dislocations energy were not considered in their calculations. These terms have a great impact especially in specimens with high density of these defects and as we know mechanical milling process reduces the grain size and increase the grain boundary and dislocation densities.

3.2. Experimental results

The XRD patterns of the milled powders (0 h, 50 h, 110 h and 180 h) have been shown in Fig. 6. The intensity of nickel peaks are stronger than titanium ones in raw material which is due to higher atomic number and hence higher scattering factor of nickel than titanium. The peaks of both nickel and titanium became broader and their intensities decreased as the milling process continued. Reduction of crystallite size and internal strain increasing due to mechanical deformation of powders and high amounts of defects caused these changes in XRD patterns of milled samples. It seems that nickel peaks have shifted to higher angles with increasing in milling time. Two reasons have been mentioned for this shift to the higher angles: first, dissolution of smaller substitutional atoms than solvent atoms. In case of mechanical milling, impurities like iron atoms from balls and milling container dissolve in nickel lattice and their amounts increase with milling. The amount of iron contamination after 180 h milling was reported about 1 at.% using AES analysis which contract the lattice and cause peaks shift to the higher angles [21]. The other reason for peak shift to the right in the XRD pattern is stacking faults. Heavy cold deformation in f.c.c metals introduces stacking faults on (111) planes which cause shift of this peak to the higher angles [21].

The XRD pattern of 50 h milled sample shows an intensity increasing in (002) titanium peak which is even more intense than (101) peak. Actually this increment is due to partially transformation of titanium α to metastable titanium ω during mechanical milling and severe plastic deformation of titanium. In other words, the ω -phase titanium peak in XRD pattern of 50 h milled sample overlap (002) titanium α peak. Pilarczyk et al. [22] have reported the same increment in (002) titanium peak after mechanical alloying of Ni and Ti powders but they reported no reason for this phenomenon. Todaka et al. [23] reached the ω -phase metastable titanium by repeated high pressure torsion straining of pure titanium. They have explained this metastable ω -phase transform to α -phase at 150 °C. That is why the ω -phase peak has been disappeared in longer milled samples. Rising temperature due to milling process has accelerated the reverse transform of ω -phase titanium to α -phase.

The XRD pattern of 110 h milled sample reveals that Ni and Ti elements are still present in the specimen and it seems 110 h milling was not enough for production of NiTi solid solution or amorphous structures. Although Miedema's semi empirical method shows that amorphous phase has lower Gibbs free energy than solid solution structure after 110 h (20 nm crystallite size and 0.5% lattice strain), the

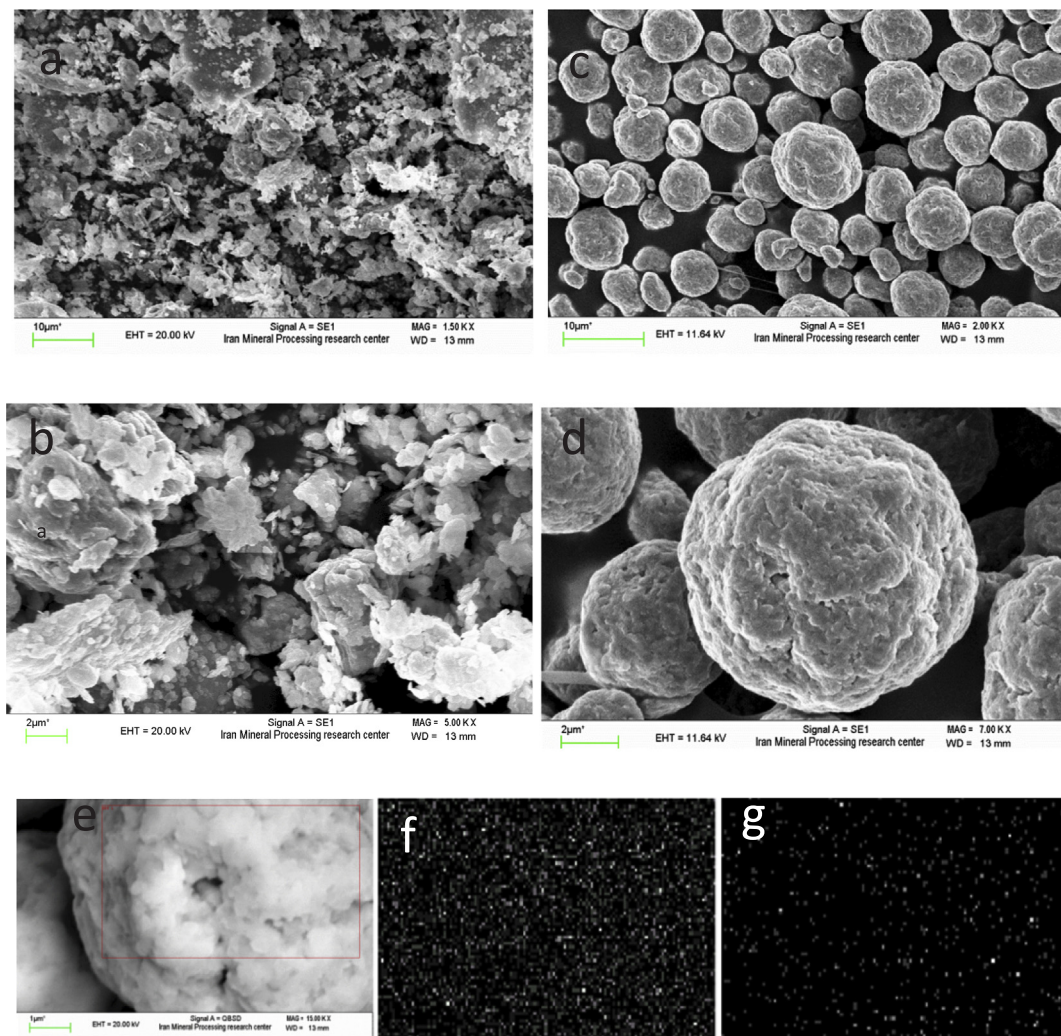


Fig. 8. SEM micrographs of milled samples: (a) and (b) after 110 h milling, (c), (d) and (e) after 180 h milling, (f) and (g) EDS elemental map of Ni and Ti respectively in area specified in (e).

XRD pattern introduces only Ti and Ni elements after 110 h milling. It means the energy of milling process after 110 h was not enough to conquer the activation energy of NiTi solid solution or amorphous formation.

After 180 h milling, all peaks of Ni and Ti elements disappeared and a halo pattern formed which indicates formation of an amorphous phase, as the other researchers have reported [6,24–26]. It is clear that further milling up to 180 h, would not lead to formation of solid solution because the lattice defects increase with mechanical milling process [21]. These results confirm thermodynamic calculations which introduced the amorphous phase as the product stable phase of milled Ni and Ti powders.

Fig. 7 shows the variations of crystallite size and lattice strain of nickel milled powders until 110 h using Williamson-Hall equation and XRD patterns of milled samples. It is clear that the crystallite size of nickel dropped off considerably by increasing in milling time but it tends to a constant value which further refinement will not happen. This crystallite size refinement can be explained by studying of dislocations in milled samples. There are three main reasons for activation of dislocation locking mechanism and hardness increasing in milled samples: 1) Arriving of titanium atoms into the nickel lattice and formation of solid solution, 2) the dislocation density increment due to hard working effect of mechanical milling and 3) segregation of titanium atoms in the stacking faults of nickel. Equation (11) shows the linear relation between hardness and minimum distance between two

adjacent dislocations in a pile up. In short, mechanical milling increases dislocation density and hardness and decreases the minimum distance between two dislocations in a pile up and this small distances lead to the formation of low angle grain boundaries and eventually smaller crystals [19,27–29].

$$L = 3Gb/\pi(1 - \nu)h$$

where (L) is the minimum distance between two dislocations in a pile up, (G) is the shear modulus, (b) is the burgers vector, (ν) is the Poisson ratio and (h) is the hardness.

The lattice strain of nickel increases during milling process. It is due to increasing in lattice defects density and specifically dislocation density. Dissolution of titanium or iron atoms in nickel and distortion of nickel lattice is another reason for lattice strain increasing in Fig. 7.

SEM images and elemental mapping of the powders have been shown in Fig. 8. As it can be seen from Fig. 8 (a) and (b), the morphology of milled powders after 110 h changed to the flaked-like shape with high aspect ratio and wide range of size distribution. In ductile-milling systems like nickel and titanium, started powders get flattened to platelet shape in early stages of milling due to balls-particles collisions and plastic deformation of particles. Then these platelet particles get cold welded together and form a layer composite structure of constituents in micro-size scale. In this stage atoms can diffuse from one layer to the other because of the energy transferred from balls collisions and heat increasing due to milling process. Except the

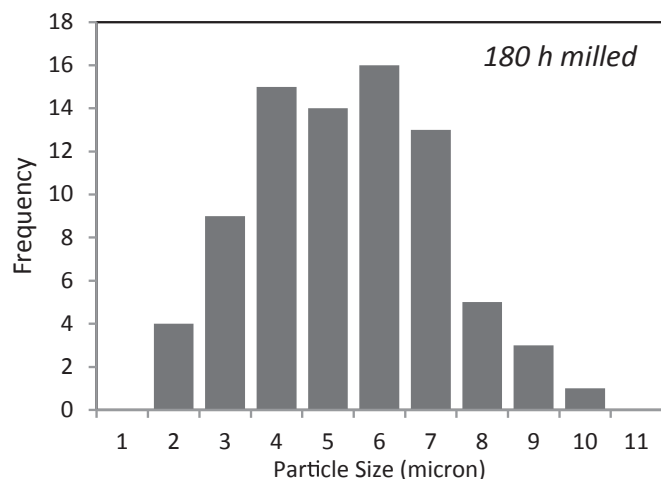


Fig. 9. Particle size distribution of 180 h milled sample.



Fig. 10. FESEM image of 180 h milled sample.

diffusion and alloying, dislocation density increasing and work hardening of powders are other consequences of mechanical milling process. The fracturing of hardened particles overcomes cold weld process in longer milling times and finally particles get a spherical morphology with a narrow size distribution (Fig. 9). Fig. 8-(c) and (d) show the morphology of powders after 180 h milling which has reached this stage and the uniform distribution of nickel and titanium in Fig. 8-(f) and (g) shows completion of alloying process. But these spherical particles are made of smaller grains as it can be seen from FESEM image of 180 h milled sample in Fig. 10.

Fig. 11 shows the XRD pattern of 180 h milled powders after heat treatment at 950°C for 20 min under argon atmosphere. The results show the formation of austenite B_2 NiTi (marked with letter A at 42.5°), Ni_3Ti and $NiTi_2$ intermetallic compounds after heat treatment. The formation of intermetallic compounds after heat treatment is due to lower Gibbs free energy of these compounds than amorphous and solid solution. Besides, amorphous structure after mechanical milling process and high temperature during heat treatment accelerate diffusion of titanium atoms and it leads to the formation of intermetallic compounds.

4. Conclusions

The original Miedema's semi empirical method anticipated two Ni–Ti solid solutions with 28 at.% Ni and 63 at.% Ni as phases with lower Gibbs free energy compared with amorphous phase. But considering the energies of dislocations and grain boundaries (which have

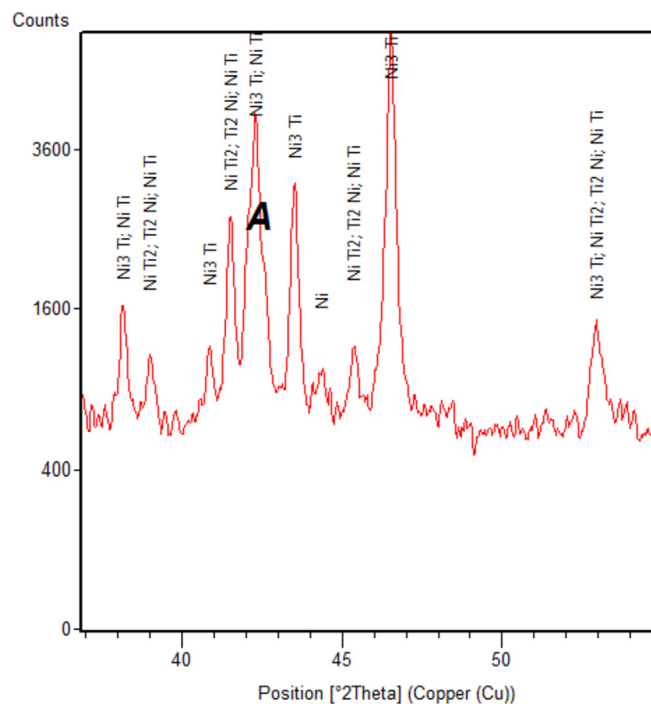


Fig. 11. XRD pattern of Ni–Ti sample after 180 h milling and heat treatment.

high densities in milled samples) shifted the solid solution curve up to the amorphous one. Thus, amorphous phase reached lower Gibbs free energy than nanostructured solid solution. In short, mechanical milling process leads to the stability of amorphous phase which is in agreement with XRD results of milled Ni–Ti powders after 180 h. The SEM micrographs of 110 h milled Ni–Ti powders showed a flaked-like morphology with wide range of particle size while the 180 h milled micrographs showed a spherical morphology with narrow particle size distribution and homogenous distribution of Ni and Ti which indicates the final stage of milling in Ni–Ti system. The intermetallic compounds (B_2 NiTi, Ni_3Ti and $NiTi_2$) have been formed only after heat treatment of milled powders at 950°C which shows the diffusion of titanium atoms into the nickel lattice during heat treatment.

Acknowledgments

The study was performed by financial supports of Iran Nanotechnology Initiative Council and their supports are greatly acknowledged.

References

- [1] T. Mousavi, M.H. Abbasi, F. Karimzadeh, Thermodynamic analysis of NiTi formation by mechanical alloying, *Mater. Lett.* 63 (2009) 786–788.
- [2] H. Hiraga, T. Inoue, S. Kamado, Y. Kojima, A. Matsunawa, H. Shimura, Fabrication of NiTi intermetallic compound coating made by laser plasma hybrid spraying of mechanically alloyed powders, *Surf. Coating Technol.* 139 (2001) 93–100.
- [3] L.L. Ye, Z.G. Liu, K. Raviprasad, M.X. Quan, M. Umemoto, Z.Q. Hu, Consolidation of MA amorphous NiTi powders by spark plasma sintering, *Mater. Sci. Eng.* 241 (1998) 290–293.
- [4] R. Amini, F. Alijani, M. Ghaffari, M. Alizadeh, A.K. Okyay, Formation of B_{19}' , B_2 , and amorphous phases during mechano-synthesis of nanocrystalline NiTi intermetallics, *Powder Technol.* 253 (2014) 797–802.
- [5] A. Takasaki, Mechanical alloying of the Ti–Ni system, *Phys. Stat. Sol.* (1998) 183–191.
- [6] R.B. Schwarz, R.R. Petrich, C.K. Saw, The synthesis of amorphous Ni–Ti alloy powders by mechanical alloying, *J. Non-Cryst. Solids* 76 (1985) 281–302.
- [7] A.K. Niessen, A.R. Miedema, F.R. de Boer, R. Boom, Enthalpies of formation of liquid and solid binary alloys based on 3d metals IV. alloys of Cobalt, *Physica B* 151 (1988) 401–432.
- [8] A.K. Niessen, A.R. Miedema, F.R. de Boer, R. Boom, Enthalpies of formation of liquid and solid binary alloys based on 3d metals V. alloys of Nickel, *Physica B* 152 (1988) 303–346.

- [9] H. Bakker, G.F. Zhou, H. Yang, Mechanically driven disorder and phase transformations in alloys, *Prog. Mater. Sci.* 39 (1995) 159–241.
- [10] A.R. Miedema, F.R. DeBoer, R. Boom, Predicting heat effects in alloys, *Physica* 103 B (1981) 67–81.
- [11] D.R. Gaskell, *Introduction to the Thermodynamics of Materials*, fifth ed., CRC press, 2008.
- [12] P.I. Loeff, A.W. Weeber, Diagrams of formation enthalpies of amorphous alloys in comparison with the crystalline solid solution, *J. Less Common. Met.* 140 (1988) 299–305.
- [13] S. Sheibani, S. Heshmati-Manesh, A. Ataie, Structural investigation on nano-crystalline Cu–Cr supersaturated solid solution prepared by mechanical alloying, *J. Alloy. Comp.* 495 (2010) 59–62.
- [14] W.F. Gale, T.C. Totemeier, *Smithells Metals Reference Book*, eighth ed., Elsevier Butterworth-Heinemann, 2004.
- [15] N.K. Mukhopadhyay, D. Mukherjee, S. Bera, I. Manna, R. Manna, Synthesis and characterization of nano-structured Cu–Zn γ -brass alloy, *Mater. Sci. Eng.* 485 (2008) 673–680.
- [16] G.E. Dieter, *Mechanical Metallurgy*, third ed., McGraw-Hill, 1976.
- [17] D. Hull, *Introduction to Dislocations*, Pergamon Press, Oxford, 1965.
- [18] G.K. Williamson, R.E. Smallman, Dislocation densities in some annealed and cold worked metals from measurements on the X-ray Debye-Scherrer spectrum, *Philos. Mag. A* 1 (1956) 34–46.
- [19] G.H.A. Bagheri, The effect of reinforcement percentages on properties of copper matrix composites reinforced with TiC particles, *J. Alloy. Comp.* 676 (2016) 120–126.
- [20] L.E. Murr, *Interfacial Phenomena in Metals and Alloys*, Addison-Wesley publishing company, 1975.
- [21] C. Suryanarayana, Mechanical alloying and milling, *Prog. Mater. Sci.* 46 (2001) 1–184.
- [22] W. Pilarczyk, R. Nowosielski, A. Pilarczyk, P. Sakiewicz, A production attempt of Ni₅₀Ti₅₀ and Ni₅₂Ti₄₁Nb₇ alloys by mechanical alloying method, *Mater. Sci. Eng.* 47 (2011) 19–26.
- [23] Y. Todaka, J. Sasaki, T. Moto, M. Umemoto, Bulk submicrocrystalline ω -Ti produced by high-pressure torsion straining, *Scripta Mater.* 59 (2008) 615–618.
- [24] B.S. Murty, S. Ranganathan, M. Mohan Rao, Solid state amorphization in binary Ti–Ni, Ti–Cu and ternary Ti–Ni–Cu system by mechanical alloying, *Mater. Sci. Eng. A* 149 (1992) 231–240.
- [25] W. Maziarz, J. Dutkiewicz, J. Van Humbeeck, T. Czeppe, Mechanically alloyed and hot pressed Ni–49.7Ti alloy showing martensitic transformation, *Mater. Sci. Eng. A* 375–377 (2004) 844–848.
- [26] J. Eckert, L. Schultz, K. Urban, Synthesis of Ni–Ti and Fe–Ti alloys by mechanical alloying: formation of amorphous phases and extended solid solutions, *J. Non-Cryst. Solids* 127 (1991) 90–96.
- [27] J. Eckert, Relationships governing the grain size of nanocrystalline metals and alloys, *Nanostruct. Mater.* 6 (1995) 413–416.
- [28] J. Eckert, I. Borner, Nanostructure formation and properties of ball-milled NiAl, *Mater. Sci. Eng. A* 239–240 (1997) 619–624.
- [29] C.C. Koch, The synthesis and structure of nanocrystalline materials produced by mechanical attrition: a review, *Nanostruct. Mater.* 2 (1993) 109–129.